Deterministic numerical model for treating the three elastic constants in nematic liquid-crystalline polymers

Houjie Tu, Gerhard Goldbeck-Wood, and Alan H. Windle
Department of Materials Science and Metallurgy, University of Cambridge, Cambridge CB2 3QZ, United Kingdom
(Received 18 September 2000; published 18 June 2001)

In this paper, a deterministic model, which considers the three Frank elastic constants, is introduced. It is based on a lattice model and a director is used to represent the orientation of the liquid crystals in each cell. A tensor expression of the so-called ''texture field'' is deduced so that the nematic symmetry is conserved automatically. In the current model, the evolution of the director field can be viewed as a process towards the state of zero elastic torque. The model forms the basis for an improved understanding of the mesoscale structures and rheological phenomena of nematic liquid-crystalline polymers. It has been tested in its ability to reproduce the Fréedericksz transitions, and simulations of thin liquid crystalline polymer films clearly show the effect of unequal elastic constants on the director microstructure evolution.

DOI: 10.1103/PhysRevE.64.011704 PACS number(s): 61.30.Gd, 61.30.Jf, 61.30.Cz

I. INTRODUCTION

The texture evolution of liquid-crystalline polymers (LCP's) in external fields is of significant scientific and industrial interest, and considerable effort has been invested in understanding the orientation field, both experimentally and numerically. Although modeling has contributed significantly to an improved understanding of this complex process [1–12], existing three-dimensional models fall short of the requirements for a realistic description on either or both of the following grounds: (a) they assume equal Frank elastic constants although LCP's have very different values, and (b) Monte Carlo simulations are used, which cannot be easily related to real-time evolution or deal with external fields, in particular flow fields, in a straightforward manner. In this paper, we aim to advance our ability to handle LCP structure evolution by presenting a deterministic model that includes the three Frank elastic constants as discrete entities.

From the macroscopic point of view, the orientation of a nematic liquid crystal can be described by a director field $\vec{n}(\vec{r},t)$ and the equilibrium state of the director field is characterized by a minimum of the Frank elastic free energy. The Frank elastic free-energy density of a deformed specimen relative to the nondeformed one can be expressed by the following vectorial form [13]

$$f=\tfrac{1}{2}\{k_1(\vec{\nabla}\cdot\vec{n})^2+k_2[\vec{n}\cdot(\vec{\nabla}\times\vec{n})]^2 + k_3[\vec{n}\times(\vec{\nabla}\times\vec{n})]\cdot[\vec{n}\times(\vec{\nabla}\times\vec{n})]\}, \quad (1)$$

where $\vec{n}\cdot\vec{n}=1$ and $\vec{n}$ is equivalent to $-\vec{n}$, k_1, k_2, and k_3 are the three Frank elastic constants that are associated with the three types of deformation: splay, twist, and bend, respectively. In the equilibrium state, the director $\vec{n}$ must be, at each point, parallel to the ''texture field'' $\vec{h}$ given by the functional derivative [13]

$$\vec{h}=-\frac{\delta f}{\delta\vec{n}}, \quad (2)$$

which can be split into the splay, twist, and bend components [13]

$$\vec{h}=\vec{h}_S+\vec{h}_T+\vec{h}_B, \quad (3)$$

$$\vec{h}_S=k_1\vec{\nabla}(\vec{\nabla}\cdot\vec{n}), \quad (4)$$

$$\vec{h}_T=-k_2\{A\vec{\nabla}\times\vec{n}+\vec{\nabla}\times(A\vec{n})\}, \quad (5)$$

$$\vec{h}_B=k_3\{\vec{B}\times(\vec{\nabla}\times\vec{n})+\vec{\nabla}\times(\vec{n}\times\vec{B})\}, \quad (6)$$

where $A=\vec{n}\cdot\vec{\nabla}\times\vec{n}$ and $\vec{B}=\vec{n}\times(\vec{\nabla}\times\vec{n})$.

Mesoscale lattice models have been widely used [1–4] for simulating textures and their evolution in LC's. In general, the simulations are started from the isotropic phase, in which the directors are randomly oriented. The relaxation algorithms are designed to minimize the total free energy of the system, by picking a cell at random and applying different annealing rules. According to Assender and Windle [2], a careful choice of the energy function form is essential, if the full Frank form is not used. The vectorial form of the Frank elastic free energy has been applied [4] previously to treat unequal elastic constants. In order to get the free energy, a subtly designed flip scheme was developed to treat the director symmetry, which requires that $\vec{n}$ is physically equivalent to $-\vec{n}$.

In order to deal with the nematic symmetry, Gruhn and Hess [5] proposed a model, in which the Frank free energy was expressed in a tensorial form. This means that the nematic symmetry is conserved automatically. In their model, a Monte Carlo algorithm was implemented to find the equilibrium configuration of the director field, although only two-dimensional simulation results were reported [5]. Romano [6] further investigated this pairwise additive potential proposed by Gruhn and Hess [5] using a Monte Carlo simulation. Recently, Luckhurst and Romano [7] proposed another scheme by removing the highest rank term from the expansion of the potential and it would be used to study the elastic and defect behavior of nematogens [7].

An alternative to Monte Carlo is to use the Ericksen-Leslie equation [8–10] as a basis for a deterministic relaxation algorithm. In the absence of an external field, the Ericksen-Leslie equation describing the relaxation of the director field in nematics can be expressed as

 ©2001 The American Physical Society

$$\frac{\partial \vec{n}}{\partial t} = \frac{1}{\gamma_1}(\vec{n}\times\vec{h})\times\vec{n}, \tag{7}$$

here $\vec{n}\times\vec{h}$ is the torque per unit volume due to the curvature elasticity, and γ_1 is the rotational viscosity coefficient. External torque, such as magnetic torque or viscous torque, can be included easily. Starting from a relaxation equation for the alignment tensor, Kilian and Hess [11,12] put forward an algorithm that maintains the nematic symmetry. However, only results for the case of equal constants have been reported.

In this paper, we present a deterministic model, which handles the three Frank elastic constants as discrete values. In this model, the curvature elastic torque, rather than the free energy, is used as a driving force of the evolution of the director field. Compared to the vectorial model [4], the advantage of the current model is that nematic symmetry is conserved automatically by using the tensorial expression of the elastic torque. Another advantage is that this model can be used for the numerical calculation of both the static and the dynamic behavior of the director. The paper is arranged as follows. Section II presents the derivation of the algorithm. Starting from the tensorial form of the Frank elastic free energy [5], a ''texture field'' expression in tensorial form is deduced. In Sec. III, the model is tested and calibrated by reproducing the Fréedericksz transitions. In Sec. IV the simulation results for the evolution of defects are given in the case of two-dimensional (2D) equivalent results for 3D samples, as well as the dynamical properties of the director, are described in following papers [14,15].

II. MODEL

The Frank elastic free energy can be written in the following tensorial according to Gruhn and Hess [5]

$$\begin{aligned} f = {} & \tfrac{1}{2}[\tfrac{1}{2}k_2\nabla_\lambda n_\mu n_\nu \nabla_\lambda n_\mu n_\nu + (k_1-k_2)\nabla_\lambda n_\lambda n_\mu \nabla_\nu n_\nu n_\mu \\ & + \tfrac{1}{2}(k_3-k_1) n_\mu n_\nu \nabla_\mu n_\lambda n_\kappa \nabla_\nu n_\lambda n_\kappa], \end{aligned} \tag{8}$$

which is equivalent to Eq. (1) except for surface terms [16]. Here the Greek subscripts refer to the Cartesian components, for which the summation convention is used, and

$$\nabla_\alpha = \frac{\partial}{\partial x_\alpha}, \quad \vec{r} = (x_1, x_2, x_3) = (x, y, z).$$

In fact, we propose a tensorial form, which is exactly equivalent to Eq. (1) including the surface terms

$$\begin{aligned} f = {} & \tfrac{1}{2}[\tfrac{1}{2}k_2(\nabla_\lambda n_\mu n_\nu \nabla_\lambda n_\mu n_\nu - \nabla_\lambda n_\mu n_\nu \nabla_\nu n_\mu n_\lambda) \\ & + k_1 \nabla_\lambda n_\lambda n_\mu \nabla_\nu n_\nu n_\mu \\ & + \tfrac{1}{2}(k_3-k_1) n_\mu n_\nu \nabla_\mu n_\lambda n_\kappa \nabla_\nu n_\lambda n_\kappa], \end{aligned} \tag{9}$$

In order to derive the texture field $\vec{h}$, which is generated by spatial inhomogeneity of the director field, note that according to Eqs. (8) and (9), the Frank elastic free energy is a function of the tensor $\vec{n}\vec{n}$ and its gradients $\nabla\vec{n}\vec{n}$, i.e.,

$$f = f(n_\beta n_\gamma, \nabla_\alpha n_\beta n_\gamma). \tag{10}$$

We impose a small variation $\delta(n_\beta n_\gamma)$ at all points:

$$\delta f = \int \left\{ \frac{\partial f}{\partial n_\beta n_\gamma}\delta(n_\beta n_\gamma) + \frac{\partial f}{\partial \nabla_\alpha n_\beta n_\gamma}\nabla_\alpha(\delta n_\beta n_\gamma) \right\} d\vec{r}. \tag{11}$$

Integrating the second term by parts and neglecting the surface terms

$$\delta f = \int \left\{ \frac{\partial f}{\partial n_\beta n_\gamma} - \nabla_\alpha\left(\frac{\partial f}{\partial \nabla_\alpha n_\beta n_\gamma} \right) \right\} \delta(n_\beta n_\gamma)\, d\vec{r}. \tag{12}$$

Now considering the symmetry of the tensor

$$\delta f = 2\int n_\gamma \left\{ \frac{\partial f}{\partial n_\beta n_\gamma} - \nabla_\alpha\left(\frac{\partial f}{\partial \nabla_\alpha n_\beta n_\gamma} \right) \right\} \delta n_\beta\, d\vec{r}. \tag{13}$$

By comparing Eq. (12) with Eq. (2), we find

$$h_\beta = 2 n_\gamma f_{\beta\gamma}, \tag{14}$$

$$f_{\beta\gamma} = \nabla_\alpha\left(\frac{\partial f}{\partial \nabla_\alpha n_\beta n_\gamma} \right) - \frac{\partial f}{\partial n_\beta n_\gamma}. \tag{15}$$

In the presence of an external field, the evolution of the directors is governed by the following Ericksen-Leslie or Nemato-dynamic [13] equation:

$$\begin{aligned} \frac{\partial \vec{n}}{\partial t} + \vec{\nu}\cdot\boldsymbol{\nabla}\vec{n} = {} & \vec{n}\cdot\boldsymbol{\Omega} + \lambda(\boldsymbol{\Gamma}\cdot\vec{n} - \Gamma{:}\vec{n}\vec{n}\vec{n}) \\ & + \frac{1}{\gamma_1}\{\vec{h} + \chi\vec{n}\cdot\vec{H}\vec{H} - [\vec{h}\cdot\vec{n} + \chi(\vec{n}\cdot\vec{H})^2]\vec{n}\}, \end{aligned} \tag{16}$$

where $\boldsymbol{\Gamma}$ and $\boldsymbol{\Omega}$ are the symmetric and antisymmetric parts of the velocity ($\vec{\nu}$) gradient tensor, which represents the extensional and rotational effect, respectively, $\vec{H}$ and χ are the magnetic field and susceptibility, respectively, and λ is the tumbling parameter.

According to Beris and Edwards [16], $f_{\beta\gamma}$ should be symmetric and traceless. The ''texture field'' $\vec{h}$, given by Eqs. (14) and (15), is found to take the following form:

$$\begin{aligned} h_\beta = 2 n_\alpha \{ & k_2 \Delta n_\alpha n_\beta + (k_1-k_2)[\nabla_{\alpha\gamma} n_\gamma n_\beta + \nabla_{\beta\gamma} n_\gamma n_\alpha \\ & - \tfrac{2}{3}\delta_{\alpha\beta}\nabla_{\gamma\lambda} n_\gamma n_\lambda] + (k_3-k_1)[\nabla_\gamma(n_\gamma n_\lambda \nabla_\lambda n_\alpha n_\beta) \\ & - \tfrac{1}{2}\nabla_\alpha n_\gamma n_\lambda \nabla_\beta n_\gamma n_\lambda + \tfrac{1}{6}\delta_{\alpha\beta}\nabla_\gamma n_\lambda n_\mu \nabla_\gamma n_\lambda n_\mu]\}, \end{aligned} \tag{17}$$

where $\nabla_{\alpha\beta} = \partial^2/\partial x_\alpha \partial x_\beta$.

This final expression can in fact be deduced from either Eqs. (8) or (9), with exactly the same result. If $k_1 = k_2$

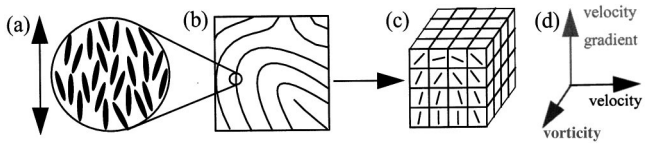

FIG. 1. A schematic representation of the lattice model. The liquid crystal is subdivided into cubic cells. Each cell has a director and the director is the average orientation of the long axes of the molecules within the cell.

$=k_3$, Eq. (17) is reduced to the one-constant form, which was used by Kilian and Hess [11].

Equations (16) and (17) describe the relaxation of the director field. For a given initial pattern and boundary conditions, Eq. (16) can be integrated numerically by standard techniques.

The director field of an LCP is represented by a set of directors in the cells of a spatially fixed cubic lattice as shown in Fig. 1. A normal finite difference scheme is adopted for discretising the Ericksen-Leslie equation (16). Starting from a given director pattern and boundary conditions, the evolution of the director field can be simulated.

III. REPRODUCING THE FRÉEDERICKSZ TRANSITIONS

In order to ascertain that the model can differentiate the three types of distortions, the Fréedericksz transitions [17] have been simulated. The Fréedericksz transitions occur when an electric or magnetic field ($\vec{H}$) is applied to an LC cell that is constrained by fixed boundary conditions at two parallel plates. If the magnetic field is perpendicular to the easy axis of the directors ($\vec{e}$), the pure Fréedericksz transitions can occur. When a magnetic field $\vec{H}\perp\vec{e}$ is applied, the equilibrium uniform state, in which the directors are all aligned along the easy axis, remains unchanged as long as the strength is less than the critical-field strength H_c. If $H>H_c$, the directors lose their stability and bifurcation of the stable states develops, leading to a tilt of the directors towards the magnetic-field direction. By defining suitable boundary conditions of two plates and the direction of the applied field, only one type of distortion is activated at the onset of the transition. So the threshold H_c is only related to the elastic constant corresponding with that distortion. The threshold value is given by [17]

$$H_c=\frac{\pi}{d}\left(\frac{k_i}{\chi}\right)^{1/2}, \tag{18}$$

where $i=1,2,3$, respectively, and d is the thickness of the LC cell. Figure 2 shows a diagram of these three typical geometries.

Based on the theoretical solutions, the Fréedericksz transitions have been successfully applied to measure the Frank elastic constants experimentally for small molecular weight liquid crystals. Here the simulation of the Fréedericksz transitions are used as a test of the effect of differentiation of the three elastic constants in the model.

Hobdell and Windle [4] simulated the Fréedericksz transitions by including an additional energy term that reflected

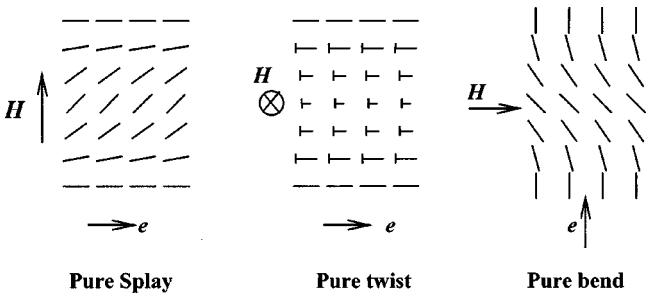

FIG. 2. The schematic representation of the three geometries of the Fréedericksz transitions: (a) pure splay, (b) pure twist, and (c) pure bend transitions. The initial pattern is a monodomain that is imposed by the boundary conditions. $\vec{H}$ is the external magnetic field, its direction is perpendicular to the initial director. The directors are initially parallel to $\vec{e}$.

the effect of a magnetic field. The results reported [5] were consistent with the theoretical prediction. It is quite straightforward to use the current algorithm to simulate the Fréedericksz transitions. In a quiescent state ($\vec{\nu}=0$) but including the magnetic torque, the governing equation has the following form:

$$\frac{\partial\vec{n}}{\partial t}=\frac{1}{\gamma_1}\{\vec{h}+\chi\vec{n}\cdot\vec{H}\vec{H}-[\vec{h}\cdot\vec{n}+\chi(\vec{n}\cdot\vec{H})^2]\vec{n}\}. \tag{19}$$

The following calculations have been performed on a $20\times20\times20$ lattice and the strength of magnetic field has been normalized by H_c.

A. Twist transitions

As a result of symmetry, the twist angle reaches its maximum value at the middle plane. The maximum twist angle ϕ_m can be obtained by the following equation [17]:

$$\frac{H}{H_c}=\frac{2}{\pi}\int_0^{\pi/2}\frac{d\Psi}{(1-\sin^2\phi_m\sin^2\Psi)^{1/2}}. \tag{20}$$

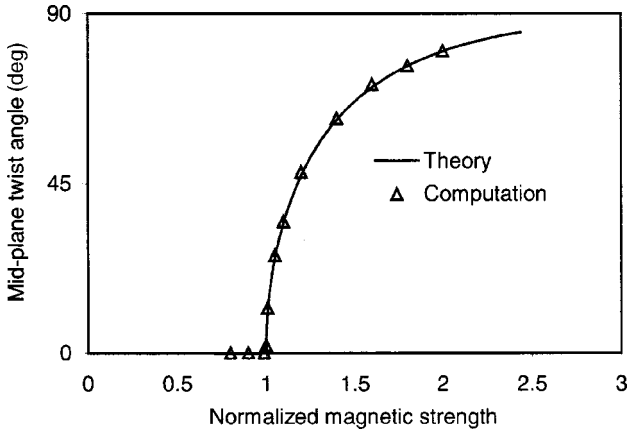

FIG. 3. The twist angles of the directors on the midplane versus the magnetic-field strength for the pure twist transition. The continuous line is the analytical result, the point the computational result.

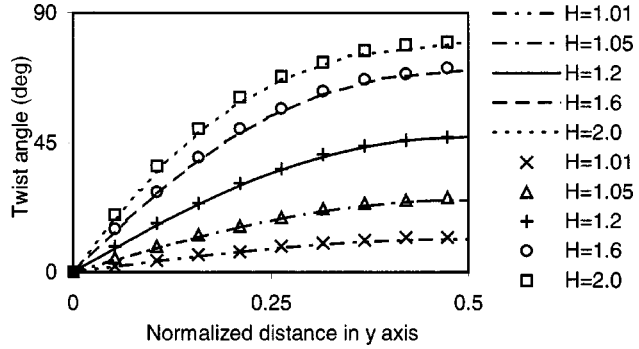

FIG. 4. The twist angles of the directors in the different layers for the pure twist transition. Lines and points indicate analytical and computational results, respectively.

The distribution of the twist angles along the thickness direction (y) is determined by [17]

$$\frac{H}{H_c}\frac{y}{d}=\frac{1}{\pi}\int_0^{\phi}\frac{d\Psi}{(\sin^2\phi_m-\sin^2\Psi)^{1/2}},\quad 0\leqslant y\leqslant\tfrac{1}{2}d. \quad (21)$$

As shown in Figs. 3 and 4, the transitions are reproduced faithfully; the onset is at the correct field strength, and the twist angles depend on the field strength and twist constant as expected. The pure twist transition is found to be independent of k_1 and k_3. The angles of the directors on the midplane *versus* the magnetic-field strength are given in Fig. 3. We have calculated the following cases: $k_1=k_2=k_3$, $2k_1=k_2=k_3$, $0.2k_1=k_2=k_3$, $k_1=k_2=2k_3$, and $k_1=k_2=0.2k_3$, the results are exactly the same. The twist angles of the directors in different layers are given in Fig. 4.

B. Splay and bend transitions

The tilt angle reaches its maximum value at the middle plane in the cases of pure splay and bend deformation. The maximum tilt angle θ_m can be obtained by the following equation [17]:

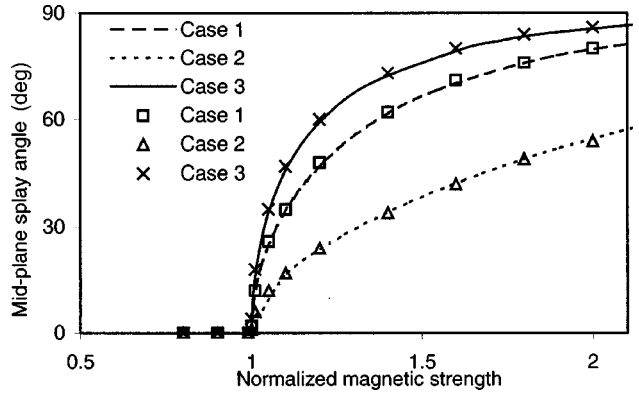

FIG. 5. The tilt angles of the directors on the midplane versus the magnetic-field strength for the pure splay transition. Lines and points indicate analytical and computational results, respectively. Cases 1, 2, and 3 refer to $k_1=k_2=k_3$, $k_1=k_2=0.2k_3$, and $k_1=k_2=2k_3$, respectively.

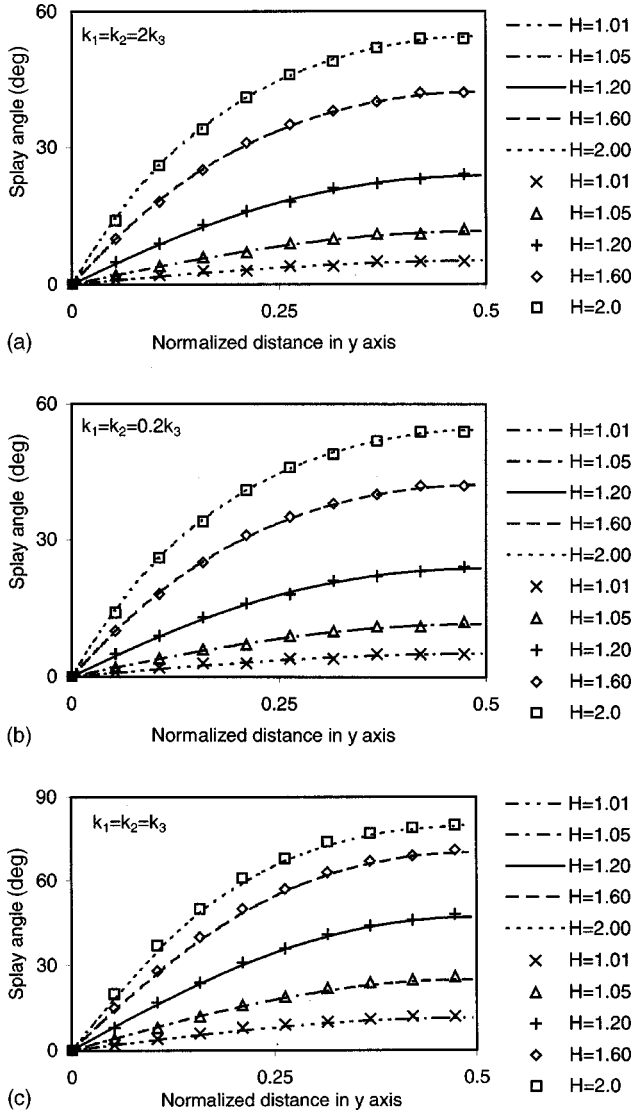

FIG. 6. The tilt angles of the directors in the different layers for the pure splay transition. Lines and points indicate analytical and computational results, respectively. (a) $k_1=k_2=2k_3$, (b) $k_1=k_2=0.2k_3$, and (c) $k_1=k_2=k_3$.

$$\frac{H}{H_c}=\frac{2}{\pi}\int_0^{\pi/2}\left(\frac{1+\varepsilon\sin^2\theta_m\sin^2\Psi}{1-\sin^2\theta_m\sin^2\Psi}\right)^{1/2}d\Psi, \quad (22)$$

where $\varepsilon=k_3/k_1-1$ represents the effect of elastic anisotropy. The distribution of the tilt angles along the y direction is determined by [17]

$$\frac{H}{H_c}\frac{y}{d}=\frac{1}{\pi}\int_0^{\theta}\left(\frac{1+\varepsilon\sin^2\Psi}{\sin^2\theta_m-\sin^2\Psi}\right)^{1/2}d\Psi,\quad 0\leqslant y\leqslant\tfrac{1}{2}d. \quad (23)$$

Figure 5 shows the angles of the directors on the midplane *versus* the magnetic-field strength in the case of the pure splay transition. Figure 6 gives the splay angles of the directors in different layers in the cases of $k_1=k_2=0.2k_3$, $k_1=k_2=2k_3$, and $k_1=k_2=k_3$, respectively. Only the results for the pure splay transitions are presented here.

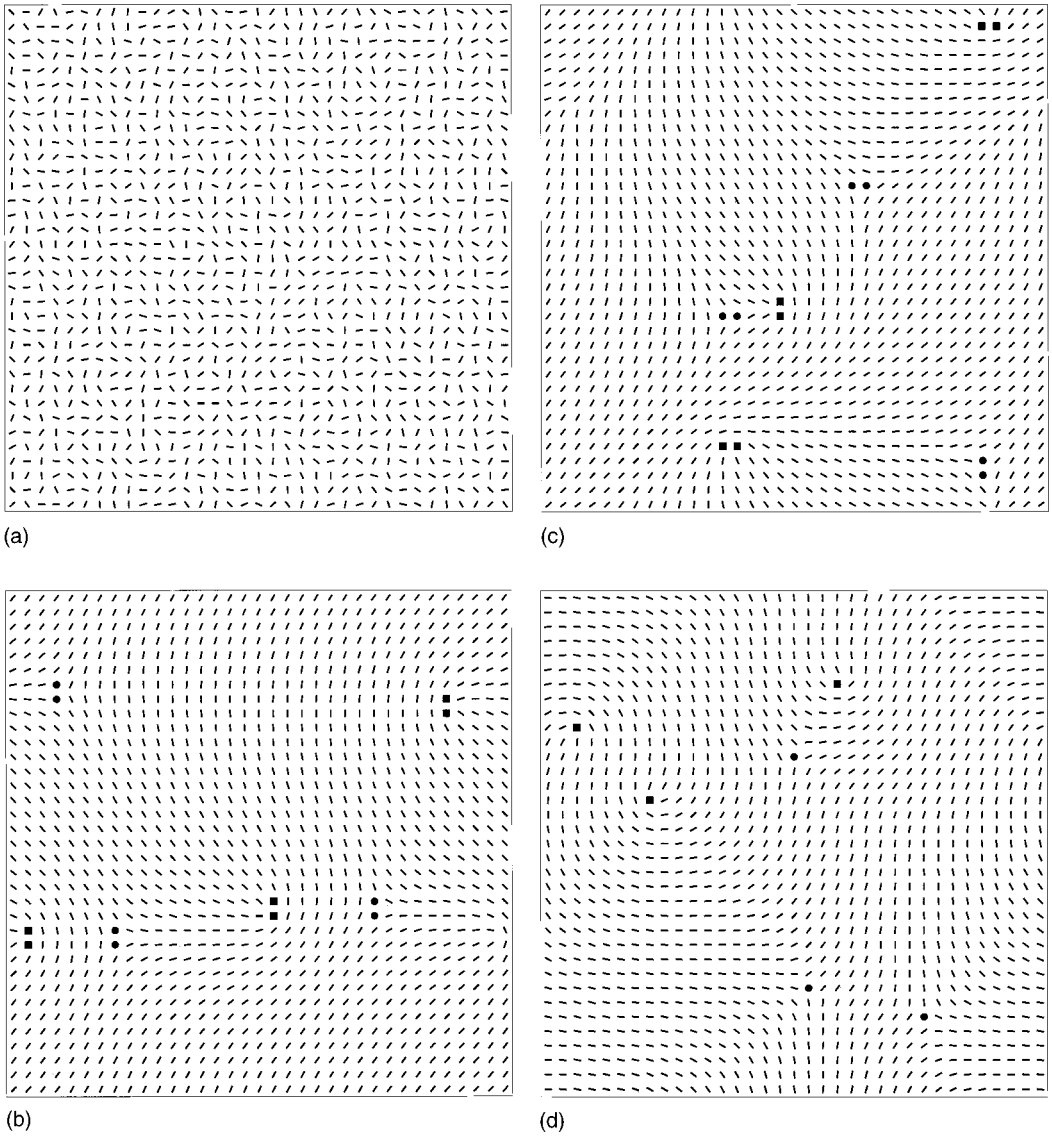

FIG. 7. Snapshots of the director fields during annealing in 2D. The defect cores, which are high free-energy cells, are indicated either by the filled squares (+1/2 defect cores) or by the filled circles (−1/2 defect cores). (a) Initial pattern in which the directors are randomly oriented, (b) $k_1=k_3$, (c) $k_1=10k_3$, and (d) $k_3=10k_1$.

The pure splay transition is independent of k_2 and depends on k_1/k_3 as predicted. Similarly, for the pure bend transition, the independence of k_2 and correct variation with k_1/k_3 have been established.

It is clear that the simulation results of the Fréedericksz transitions are in perfect agreement with the analytical solutions. This convincing test builds the confidence to simulate the microstructure in nematics with unequal elastic constants. As an example, the following section presents simulations of the annealing of a nematic thin film.

IV. DIRECTOR ANNEALING

The director structure of thin film of LCP's can be observed experimentally by special imaging techniques [18,19]. Since these observations are used for a determination of the elastic anisotropy of a material, a detailed understanding of the expected director field is required.

As a further step to examine the performance of this deterministic tensor algorithm, it has been applied to topological defects in two dimensions, according to thin-film geometry. The relaxation algorithm in 2D is the same as that in 3D described in Sec. II, and the tensorial form of the Frank elastic free energy is reduced to

$$\begin{aligned} f=&\tfrac{1}{2}k_1[(n_2\nabla_1 n_1 n_1-n_1\nabla_2 n_1 n_1)^2 \\ &+(n_2\nabla_1 n_1 n_2-n_1\nabla_2 n_1 n_2)^2] \\ &+\tfrac{1}{2}k_3[(n_1\nabla_1 n_1 n_1+n_2\nabla_2 n_1 n_1)^2 \\ &+(n_1\nabla_1 n_1 n_2+n_2\nabla_2 n_1 n_2)^2]. \end{aligned} \tag{24}$$

Considering the symmetry, Eq. (14) becomes

$$h_1 = 2n_1 f_{11} + 2n_2 f_{12}, \tag{25}$$

$$h_2 = 2n_1 f_{12} - 2n_2 f_{11}, \tag{26}$$

where

$$\begin{aligned} f_{11} = {} & k_1(n_2 n_2 \nabla_{11} n_1 n_1 + n_1 n_1 \nabla_{22} n_1 n_1 - 2n_1 n_2 \nabla_{12} n_1 n_1) \\ & + k_3(n_1 n_1 \nabla_{11} n_1 n_1 + n_2 n_2 \nabla_{22} n_1 n_1 + 2n_1 n_2 \nabla_{12} n_1 n_1) \\ & + \tfrac{1}{2}(k_3 - k_1)[(\nabla_2 n_1 n_2 + \nabla_1 n_1 n_1)^2 \\ & - (\nabla_1 n_1 n_2 - \nabla_2 n_1 n_1)^2], \end{aligned} \tag{27}$$

$$\begin{aligned} f_{12} = {} & k_1(n_2 n_2 \nabla_{11} n_1 n_2 + n_1 n_1 \nabla_{22} n_1 n_2 - 2n_1 n_2 \nabla_{12} n_1 n_2) \\ & + k_3(n_1 n_1 \nabla_{11} n_1 n_2 + n_2 n_2 \nabla_{22} n_1 n_2 + 2n_1 n_2 \nabla_{12} n_1 n_2) \\ & + (k_3 - k_1)(\nabla_2 n_1 n_2 + \nabla_1 n_1 n_1)(\nabla_1 n_1 n_2 - \nabla_2 n_1 n_1)]. \end{aligned} \tag{28}$$

In two dimensions, only the splay and the bend distortions occur. The simulation should show the effect of splay and bend elastic anisotropy on the distortions.

Figure 7 gives the typical patterns during the process of director annealing. The periodic boundary conditions are used in all of the boundaries. No external field is applied and the initial pattern is a random distribution of the directors as shown in Fig. 7(a). Figures 7(b), 7(c), and 7(d) are snapshots of the director field in the case of $k_1 = k_3$, $k_1 = 10k_3$, and $k_3 = 10k_1$ respectively. The snapshots show that the distortions around $+1/2$ defects depend on the elastic anisotropy. In the case of equal constants, i.e., no elastic anisotropy [Fig. 7(b)], the distortions of bend and splay are balanced. If the bend constant is smaller than the splay constant [Fig. 7(c)], the distortion around $+1/2$ defect core is mainly bend type, showing an archway structure. If the splay constant is smaller than the bend constant [Fig. 7(d)], the splay distortion around $+1/2$ defect core is favored and tends to a sunrise shape. The geometry shape of the $-1/2$ disclinations, on the other hand, is insensitive to the Frank elastic constants. These simulation results are in good agreement with the theoretical prediction [20] and previous simulations [1,3] using different levels of approximation.

V. SUMMARY

A numerical model has been presented to simulate the microstructures in nematic liquid crystals. A lattice model is adopted and the director is used to represent the orientation of the liquid crystals. The evolution of the directors can be considered as finding the state where the directors are parallel to the ''texture field'' instead of finding the minimum of the elastic free energy. The elastic effect of the textures is taken into account by using a tensor expression of the elastic torque, in which the three elastic constants are included and nematic symmetry is conserved automatically.

The current model can accurately reproduce the Fréedericksz transitions. It shows the splay, twist, and bend constants are appropriately identified.

The model has been used to simulate the defect structures in thin LCP films without an external field. Starting from a randomly oriented director pattern, half-defect pairs are observed during the annealing. As expected the distortions around $+\frac{1}{2}$ defects depend considerably on the elastic anisotropy.

We conclude that the current model can treat the effect of elasticity in full accord with the theoretical basis. The test results reported here confirm its behavior. The simulation results of the static and dynamic behavior of LCP's are given in two papers to follow [14,15].

ACKNOWLEDGMENT

The authors would like to acknowledge support by the EPSRC grant under its ''Processing of conventional structural materials'' program.

[1] S. E. Bedford and A. H. Windle, Liq. Cryst. **15**, 31 (1993).
[2] H. E. Assender and A. H. Windle, Macromolecules **27**, 3439 (1994).
[3] A. H. Windle, H. E. Assender, and M. S. Lavine, Proc. R. Soc. London, Ser. A **348**, 73 (1994).
[4] J. Hobdell and A. H. Windle, Liq. Cryst. **23**, 157 (1997).
[5] T. Gruhn and S. Hess, Z. Naturforsch., A: Phys. Sci. **51a**, 1 (1996).
[6] S. Romano, Int. J. Mod. Phys. B **12**, 2305 (1998).
[7] G. R. Luckhurst and S. Romano, Liq. Cryst. **26**, 871 (1999).
[8] C. Denniston, Phys. Rev. B **54**, 6272 (1996).
[9] G. Derfel, Liq. Cryst. **24**, 829 (1998).
[10] A. Kilian, Phys. Rev. E **50**, 3774 (1994).
[11] A. Kilian and S. Hess, Z. Naturforsch., A: Phys. Sci. **44a**, 693 (1989).
[12] A. Kilian and S. Hess, Liq. Cryst. **8**, 465 (1990).
[13] P. G. De Gennes and J. Prost, *The Physics of Liquid Crystals* (Clarendon, New York, 1993).
[14] H. Tu, G. Goldbeck-Wood, and A. H. Windle (unpublished).
[15] H. Tu, G. Goldbeck-Wood, and A. H. Windle (unpublished).
[16] A. N. Beris and B. J. Edwards, *Thermodynamics of Flowing Systems with Internal Microstructure* (Oxford University Press, New York, 1994).
[17] G. Vertogen and W. H. deJeu, *Thermotropic Liquid Cyrstals* (Springer-Verlag, New York, 1988).
[18] S. E. Hudson and E. L. Thomas, Phys. Rev. Lett. **62**, 1993 (1989).
[19] W. Song, X. Fan, A. H. Windle, X. Chen, and R. Qian (unpublished).
[20] G. S. Ranganath, Mol. Cryst. Liq. Cryst. **97**, 77 (1983).